Study on filling material strength and dam failure characteristics of loess dam

Nengyuan Chen
Changan University: Chang'an University
Danni Zhao
Changan University: Chang'an University
Xiong Wu
Changan University: Chang'an University
jiangbo xu (xujiangbo@yeah.net)
Chang'an University https://orcid.org/0000-0003-1567-0931
Yalin Nan
China Electronic research institute of engineering investigations and design
Ligang Niu
china electronic research institute of engineering investigations and design

Research Article

Keywords: unsaturated remolded loess, failure characteristics, confining pressure, water content, dry density

Posted Date: April 5th, 2022

DOI: https://doi.org/10.21203/rs.3.rs-1222795/v1

Abstract

Due to the special material of the loess, it is characterized by large pores and collapsibility. When the water content is low, the strength is high. However, as the water level increases after the loess dam, the soil inside the dam is continuously wetted by water. The moisture content gradually increases, some characteristics of the soil change, and the control of the dry density during construction also affects the soil properties. In this paper, the filling materials of a loess dam in Ansai, Yan'an City, Shaanxi Province were selected as the research object which is ML in the USCS classification of Loess. The effects of confining pressure, water content, and dry density on the failure characteristics and strength characteristics of unsaturated remolded loess were investigated by triaxial apparatus, while prepared soil samples at a particular water content and perform the CU(Consolidated Undrain) tests. It is found that the remolded loess samples under the conditions of low confining pressure, low water content, and high dry density show brittle failure, and obvious shear planes are formed. The stress-strain curve shows a strong strain-softening type and exhibits shear dilatancy characteristics. The unsaturated remolded loess under high confining pressure, high water content, and low dry density exhibits plastic failure and strain hardened, showing shear shrinkage phenomenon. The shear strength index of unsaturated remolded loess is affected by factors such as water content and dry density. When the dry density is kept constant, the cohesive force will decrease with the increase of water content, while the internal friction angle will decrease with the increase of water content at the lower dry density. With a dry density of 1.7g/cm 3 , the interaction between soil particles, pores and water film causes the internal friction angle to increase first, then decrease and then increase. When the water content is constant, the cohesion force will increase with the increase of dry density, and the internal friction angle will increase with the increase of dry density. Then, FLAC3D was used to conduct a numerical simulation of loess stacked dam, and it was found that with the rise of water level, the slope shear outlet of the dam with three damages gradually moved up, and the landslide volume gradually decreased, which was consistent with the on-site damage phenomenon.

1. Introduction

Loess has a wide distribution range and a large area in China (Zheng 2019). Liu (1965) completed the distribution map of loess in China and put forward the "new wind formation theory" of loess, which provides a profound theoretical basis for subsequent studies by scholars. In some engineering structures, local materials are taken into account in consideration of economic cost and other factors, which greatly saves the engineering cost. Therefore, more loess accumulation dams and siltation dams are built in northwest China for soil and water conservation. During the service of geotechnical buildings, the shear strength of filling materials is relatively high in the natural state. When rain falls or groundwater flows, the soil inside is soaked by water, therefore, a lot of geological disasters are produced Lan 2005 . The change of water content after wetting will cause structural changes in the soil (Liu 2019, Yan 2018), which will change the matrix suction and stress-strain properties of the soil (Wang 2019, Wen 2014). The wetting-induced deformations of the loess included volume and shear deformations, reflecting compression and shearing behavior induced by wetting (Xing 2019). The failure behavior of the loess along a wetting path (Liang 2016) was dependent on the stress level and the loss degree of matric suction as well as the hydro-mechanical path, and could be well described by the linear form of the Mohr-Coulomb strength theory. On this basis, the threshold value of the stress level was identified, which could be used to judge whether the wetting-induced failure of the loess occurs. The threshold value of matric suction at failure was also identified to analyze the loss degree of matric suction from stable conditions to failure. The degree of humidification can generally be characterized by the volumetric water content. According to the soil-water characteristic curve, the corresponding matrix suction can be obtained under different volumetric water contents. The relationship between soil strength and deformation parameters and matrix suction can be established through experiments (Gao 2017). However, since the measurement of the matric suction is complicated and takes a long time, the effective stress parameter can be measured by the CU(Consolidated Undrain) test to establish the absorption stress curve, which is easy to apply in practice (Xing 2016).

For unsaturated loess, the duncan-zhang model is widely applied to explore the stress-strain characteristics of the soil. However, due to its own limitations, many scholars explore the parameters of unsaturated loess and modify the formula (Ni

2018, Yang 2008). When the stress-strain characteristics of soil are obtained through the test, the relationship between shear rate, confining pressure, dry density and shear strength index of soil has a strong regularity (Dang 2009, Wang 2019, Luo 2008, Dijkstra 1994), and the equation with the good fitting relationship can be established to calculate the strength of multi-dimensional loess. At the same time, With the increase of suction, the shear strength increases and the internal friction angle decreases, both of which are non-linear changes (Patil 2016,2017,2020).

The above studies are all about the influences on the strength and deformation characteristics of unsaturated loess under the conditions of controlling suction or wetting, while the influences of confining pressure, moisture content and other factors on the failure characteristics of unsaturated loess during shearing are rarely studied. In this paper, the failure characteristics of filling materials for loess dam under different confining pressures, moisture content, and dry density are explored by using GDS unsaturated triaxial apparatus and verified by in situ monitoring.

2. Laboratory Test

2.1 Methodology

The soil used for this experiment was taken from a loess accumulation dam in Ansai Nangou, Yan 'an city, Shaanxi province, which is ML in the USCS classification of Loess. Bettersize2000 laser particle size distribution instrument was used for particle analysis of dam body soil. The particle grading curve of the sample was shown in Fig. 1. Part of the soil was dried to measure the natural moisture content, and the natural weight was calculated by retrieving the ring cutter sample. The basic physical properties of dam body soil are shown in Table 1.

Table 1 Physical properties of soil specimens

water content/%	dry density/(g•cm^{-3})	specific gravity of soil	Percentage of soil particles at different particle sizes				
			0.002mm	0.002-0.075mm	0.075-0.25mm	0.25-0.5mm	0.5-2mm
14.97%	1.557	2.71	5.72	83.01	11.27	0	0

The triaxial test used GDS unsaturated soil triaxial apparatus. The range of confining pressure controller of the system is 0-1Mpa, and the axial pressure controller can provide the maximum axial pressure of 5kN. The sensor and data conversion device of the triaxial test system can automatically collect and output the data of various parameters to be tested. The sample required for this instrument is 39.1mm in diameter and 80mm in height. It is prepared by the layered compaction method. Equal mass soil is added four times. In this test, four moisture contents, namely 10%, 15%, 20% and 25%, were taken into account, and the dry densities were 1.4g/cm^3, 1.5g/cm^3, 1.6g/cm^{3}and 1.7g/cm^3, respectively. The samples were subjected to confining pressures of 50kPa, 100kPa, 150kPa and 200kPa respectively.

The remolded soil samples retrieved from the site were air-dried under natural conditions. After air-dried, the air-dried moisture content was measured. According to the formula, the water quality of the soil samples with 10% and 15% moisture content was calculated. The samples with 20% and 25% moisture content were prepared by the dripping method, that is, the soil material with 15% moisture content was pressed into the surface of the soil sample with a rubber head dropper after forming, and then sealed and marked. The samples were placed in a moisturizing tank for 48h to make water evenly distributed in the sample.

After the sample preparation is completed, the sample is installed in the GDS static triaxial apparatus, the shear rate and confining pressure are set, and the test is stopped when the shear strain variable reaches 20%.

2.2 Results and analyzation

The failure types of soil in the triaxial test are mainly divided into three types: brittle failure, plastic failure and approximate ideal plastic failure. Brittle failure and plastic failure can be divided into three types according to their stress-strain curves: strong strain softening, weak strain softening, strong strain hardening and weak strain hardening. As can be seen from Fig. 2, when the dry density is 1.7g/cm^3, the relative displacement of soil samples on the shear plane gradually decreases with the increase of confining pressure, and the penetration degree of the fracture surface also decreases. When the confining pressure is 50kPa and 100kPa, the shear plane is more obvious, and the confining pressure increases to 150kPa and 200kPa, and the shear interface is more blurred when the sample is destroyed. When confining pressure remains unchanged and dry density increases, the failure type of samples changes from plastic failure to brittle failure (Fig. 3). The soil sample with lower dry density has more pores inside, and the soil particles are overlapped with each other. The contact between the particles is mainly point-point, point-line, and the strength is low. When subjected to a small external force, the structure is destroyed and the soil particles fall into the pores. Therefore, most of the deformation during the shearing process is caused by the constant compression of the pore volume, and shearing contraction occurs during the shearing process. The increase of dry density of soil samples internal granular arrangement more closely, sample internal contact form is given priority to with mosaic structure between particles, forms are mainly: line-line and line-face, and the particles are closely attached. Therefore, the pores between the particles are less, the pore compression amount is small, and the mutual displacement between the soil particles during the shearing process causes the volume of the soil sample to increase after shearing, that is, the shear dilatancy phenomenon occurs. As shown in Fig. 4, with the increase of water content, the shear outlet at the lower end of the shear plane moves up gradually, the included angle (acute angle) between the shear plane and the horizontal plane decreases gradually, and the length of the shear plane decreases, and the sample changes from brittle failure to plastic failure.

Figure 5 shows the stress-strain curves of remolded loess under different confining pressure and dry density conditions. As the confining pressure increases, the stress-strain curve moves up and the peak strength of the sample increases. The strain hardening degree of all the samples after increasing the confining pressure is more significant than the upper confining pressure and is a strong strain hardening type under high confining pressure.

When the sample has a water content of 10%, the dry density of 1.4g/cm^{3}and 1.5g/cm^{3}are strain hardened under different confining pressure conditions; when the sample with a dry density of 1.6g/cm^3 was shear under confining pressure of 50kPa, the deviator stress remained almost unchanged with the increase of axial strain, showing an approximate ideal plastic failure characteristic.

Samples with a dry density of 1.7g/cm^3 showed different degrees of strain softening under different confining pressures. During the formation of loess, the combination and arrangement of spatial stacking of scattered particles directly affect the strength and deformation characteristics of the soil. Under the condition of low confining pressure, the confining pressure will compress the pores between the soil particles but does not change the contact mode between the skeleton elements, and the microstructure does not change significantly, so the shear strength is low. When the confining pressure gradually increases, the pores between the soil particles are compressed, and the pores of the supports formed by lapping between the coarse particles are destroyed by external forces, forming a more stable skeleton structure, so the threshold of resistance to external forces is higher, the shear strength index also rises. In the triaxial shearing process, the change of the contact mode between the particles, the change of the mutual position of the particles and the secondary structure formation process of re-engagement between the particles, the process from unstable to stable to unstable, and finally the destruction.

It can be seen from Fig. 6(a) that the peak strength increases significantly with the increase of dry density. At low confining pressure, samples with a dry density of 1.7g/cm^3 showed strong strain softening, while other dry densities all showed strain hardening under high and low confining pressure conditions, and when confining pressure remained unchanged, the strain hardening degree gradually weakened with the increase of dry density (Fig. 6(b)). The arrangement of the skeleton element parts is tighter as the dry density is increased, the inter-particle bite force and the joint force are increased, and the number of overhead pores is reduced compared with the low density. The shape variable caused by the pores during the shearing

process is small, and the deformation mainly comes from the damage that occurs after the particles are bitten to each other, so the strength is increased.

It can be seen from Fig 7 that the stress-strain curve changes significantly with the moisture content, and the peak stress of the sample decreases with the increase of the moisture content. When dry density was 1.4g/cm^3 and 1.5g/cm^3, the change of moisture content did not significantly change the failure type of the sample. When the dry density of the sample is increased to 1.6g/cm^{3}and 1.7g/cm^3, the sample changes from brittle failure to plastic failure as the water content increases, and the strain-softening type changes to the strain hardening type. When the moisture content increases, water fills the intergranular pores in the loess framework, dissolves intergranular suffusion, thickens the water film on the surface of soil particles, decreases the intergranular bonding force and the occlusal friction force, and decreases the strength.

Fig. 8-11 shows the change rule of shear strength index and moisture content and dry density. The relationship curve between the shear strength index and moisture content and dry density is drawn by using cohesion and internal friction angle as the vertical coordinate, dry density and moisture content as the horizontal coordinate respectively. The Soviet scholars divided the cohesion into two parts: the original cohesion and the solidified cohesion (Li 2013). The original cohesive force comes from electrostatic force and van der Waals force between particles. The closer the distance between particles is, the more contact points of soil particles per unit area, the greater the original cohesive force will be. When the particles are separated from each other by a certain distance, the original cohesion is completely lost. Solidification cohesion depends on the suffusion substances present between particles, such as free chlorides, iron salts, carbonates, and organic matter in the soil. When water is filled in the intergranular pores of the soil, the suffusion substances between the soil particles are dissolved, and the strength of the intergranular connection is partially lost. When the moisture content is increasing, the salt substances between the particles are continuously dissolved, until the solidification cohesion is completely lost. Therefore, when the moisture content increases to 25%, the cohesion decreases significantly compared with 10%.

The strength of the internal friction angle mainly comes from two parts: sliding friction and occlusal friction, and the former is mainly due to the rough contact surface of minerals. The occlusal friction comes from the mutual restraint between soil particles. When the moisture content increases, the water film is formed between soil particles, the particles between the movement to promote the role, when the dry density is small, within the more pore, under the effect of external force, the particles falling into a big pore after the relative sliding, although the pore filling effect, but due to the internal porous sample, cause the strength of the growth is very limited, so the overall is still showed a trend of decline. When the dry density increases, under the condition of low moisture content, although water is favorable for sliding between particles, the internal particles are closely arranged with fewer pores. After the relative displacement between particles, it falls into the pores and occludes closely with other soil particles again, so the angle of internal friction rises. When the moisture content increases to 20%, the water film between particles thickens and the lubrication effect is obvious, so the angle of internal friction decreases. When the water content is 25%, the water film dissolves a large number of suffusion substances, and the properties change, the lubrication effect decreases, and the internal friction angle increases.

3. Comparison Of Field And Numerical Simulation Results

The object of this study is located in Ansai District, Yan 'an city, Shaanxi Province. Fig. 12-13 shows the initial state of the dam. Fig. 14-16 shows the situation of the three failure sites and describes the progressive failure process of the loess accumulation dam during the whole life cycle.

The first damage is caused by the rising water level behind the dam. Under the action of hydrodynamic force, the water forms a seepage channel in the dam body, which flows to the slope side of the airside. The shear strength of the slope foot is reduced by the water soaking, so the first damage occurs. Since a large amount of rainwater infiltrates into the cracks in the top of the dam before the second damage, the pore pressure inside the dam crest increases, the effective stress decreases, the shear strength weakens, and the dam crest soil slides along the first damage surface; meanwhile, the rising water level of reservoir causes the slope surface overflow point to move up, and the soil at the overflow outlet continues to soak and soften,

and the shear strength decreases, and the second damage occurs. Under the continuous erosion of rainwater, the topsoil of the dam is continuously slipping down along the rupture surface, it is the third damage. After the third damage, the width of the dam roof gradually decreases and almost disappears completely.

Fig. 17 shows the morphological changes of the three damages of the dam slope. The different color in the figure represents three times the damage of the dam slope sliding along the sliding surface. The amount of accumulated objects produced by the three damages is gradually reduced, the shearing outlet is gradually moved upward, the angle between the shearing surface and the horizontal plane (an acute angle) is gradually reduced, and the length of the shearing surface is gradually decreased.

Under the condition of rainfall, the continuous rise of the water level of the reservoir leads to the gradual rise of the saturation line, which leads to the increase of the soil moisture content inside the dam, leading to damage. Therefore, FlAC3D is considered to perform numerical inversion for the three damages of loess stacked dam to observe the damage patterns of dam slope and the change of external displacement and internal pore pressure.

Table 2. Numerical calculation of model parameters

Assignment parameters	density/ g•cm^3	Bulk modulus /MPa	Shear modulus /MPa	Permeability coefficient /(cm/s)	Dam body cohesion /(kPa)	Internal friction angle of the dam/(°)	Foundation cohesion /(kPa)	Friction angle within the foundation/(°)
Parameter value	1559	23	9.46	2.09077×10^{-5}	10	25	20	25

The numerical model is shown in Fig. 18. The numerical model is divided into two parts. The upper part is the loess accumulation dam body, the seepage model is isotropic seepage, and the lower part is the dam foundation, and the non-seepage model is selected. At the same time, through the experimental research and analysis, it can be found that the dam body loess is a typical elastic-plastic material, so the Mohr-Coulomb elastic-plastic model is used for calculation in this simulation. The foundation length of the model is 48.36m and the height is 10m. The dam crest width of the loess stacked dam is 3.8m, the slope angle of both sides is 40°, and the dam height is 6.12m. According to the laboratory test results, the parameters of each model are selected and assigned, as shown in the table.

When the first damage occurs, the water level is 4.85m (Fig. 19, 20), and there is an obvious water level difference on both sides. Water moves through the dam body toward the surface, and the pore water pressure field is formed inside the dam body, and the seepage force along the free face direction is formed at the toe of the slope. At the same time, under the upper gravity, slope toe appears obvious stress concentration makes the soil produces plastic deformation, in the process of seepage, the plastic zone extended in the direction of dam crest, eventually become the breakthrough. Set by command when the maximum displacement of the model reaches 100mm (Figure 21), the dam body is considered to be damaged and the calculation is stopped. In the first damage, the position of the sliding surface can be determined by the maximum shear strain increment cloud map. Generally, the position with a large shear strain increment is prone to obvious failure, while the position with a small shear strain increment is less likely to fail. As shown in Fig. 22, there is an obvious arc line in the shear strain increment program, which runs from the toe of the slope to the top of the dam, that is, the potential sliding surface of the dam body. It can be observed that the maximum increment of shear strain at the toe of the slope is observed, which indicates that the slope toe is most prone to failure. Under the action of upper gravity, the dam slope slides along the failure surface to form the first damage.

According to the shear strain increment cloud map of the first failure, an arc was drawn along the shear plane during modeling to make it consistent with the shape of the sliding plane. The part above the sliding plane was removed while the rest remained unchanged. The calculation model of the second damage of the dam body is shown in Fig.23. In this calculation, the water level height of the set reservoir is 4.936m (Fig. 24). Other conditions remain unchanged. In the second

damage, it can be seen from the shear strain increment program (Fig. 26) that the crest will slide down along the failure surface, and the crest will disappear completely, consistent with the displacement program (Fig. 25). Starting from the left side of the crest, the displacement along the orange-red area will be the largest.

According to the shear strain increment cloud map of the first failure, an arc was drawn along the shear plane during modeling to make it consistent with the shape of the sliding plane. The part above the sliding plane was removed while the rest remained unchanged. The calculation model of the second damage of the dam body is shown in Fig. 27. In this calculation, the water level height of the set reservoir is 4.936m (Fig. 28). Other conditions remain unchanged. In the second damage, it can be clearly seen from the shear strain increment program (Fig. 30) that the crest will slide down along the failure surface, and the crest will disappear completely, consistent with the displacement program (Fig. 29). Starting from the left side of the crest, the displacement along the orange-red area will be the largest.

Conclusion

The failure forms of remolded loess are affected by confining pressure, moisture content, and dry density. Under the conditions of low confining pressure, low moisture content and high dry density, there is obvious shear plane and shear dilatancy. Under the conditions of high confining pressure, high moisture content and low dry density, the samples exhibited swelling failure, volume reduction and shear shrinkage.

The stress-strain curve of remolded loess will move up with the increase of confining pressure. When water content increases, the strain-softening degree of the stress-strain curve decreases and strain hardening increases. With the increase of dry density, the stress-strain curve changes from strain hardening to strain to soften.

At low dry density, the increase of water content causes the internal friction angle to decrease. However, when the dry density is 1.7g/cm^3, due to the small internal porosity, the movement of soil particles caused by external force will again make the soil particles tightly mesh. When the water content is 10% and 15%, the water film on the surface of the particles is thinner and does not play a significant role. When it is raised to 20%, the water film is thickened and the lubricating effect is more obvious; when the water content is 25%, the water film inside the sample dissolves a large amount of cemented material, and the properties change, no longer bear the lubricating effect, and at the same time resist some external force, so the internal friction angle rises. As the water content is constant, the cohesive force increases with the increase of the dry density. When the water content is constant, the cohesive force increases with the increase of the dry density, and the internal friction angle also increases with the water content.

The numerical simulation of the loess stacked dam shows that with the rise of water level behind the dam, the seepage line gradually rises, the dam slope overflow outlet and shear outlet gradually move up, and the landslide volume gradually decreases, which is consistent with the on-site failure phenomenon.

Declarations

Conflicts of Interest

The authors declare that there are no conflicts of interest regarding the publication of this paper.

Acknowledgments

This work was partially supported by the National Natural Science Foundation of China (Nos. 41790443 & 41927806); the National Key R&D Program of China (No. 2016YFC0802203); the Fundamental Research Funds for the Central Universities, CHD (300102219213); the Key R&D Program of Shaanxi Province(2018ZDXM-SF-024); the Zhejiang Collaborative Innovation Center for Prevention and Control of Mountain Geologic Hazards (PCMGH-2017-Z-01) and the Natural Science Foundation of Qinghai Province (2019-ZJ-7050).

References

1. Dang JQ, Jiang CL, Ji ZL (2009) Effects of Shear Rate on Mechanical Behavior of Structured Loess. Chinese Journal of Underground Space and Engineering 5(3):459-462.
2. Dijkstra TA, Rogers CDF, Smalley IJ, et al (1994) The loess of north-central China: Geotechnical properties and their relation to slope stability. Engineering Geology 36(3-4):153-171.
3. Gao DH, Chen ZH, Guo N, et al (2017) The influence of dry density and matric suction on the deformation and the strength characteristics of the remolded unsaturated loess soils. Chinese Journal of Rock Mechanics and Engineering 36(3):221-229.
4. Lan HX, Lee CF, Zhou CH, Martin CD (2005) Dynamic characteristics analysis of shallow landslides in response to rainfall event using GIS. Environmental Geology 47(2):254–267.
5. Liang C, Cao C, Wu S (2016) Hydraulic-mechanical properties of loess and its behavior when subjected to infiltration-induced wetting. Bulletin of Engineering Geology and the Environment 77(1):385-397.
6. Liu DS (1965), The Loess Deposits in China. SciencePress, Beijing.
7. Liu X, Zhang N, Lan HX (2019) Effects of sand and water contents on the small-strain shear modulus of loess. Engineering Geology 260(3):105202.
8. Li GX, Zhang BY, Yu YZ (2013) Soil Mechanics. Tsinghua University Press, Beijing.
9. Luo AZ (2008) Debugging of a new true triaxial apparatus and experiment study on the strength-deformation characteristic of remolded loess. Dissertation, Northwest A&F University.
10. Ni P, Mei G, Zhao Y (2018) Influence of Raised Groundwater Level on the Stability of Unsaturated Soil Slopes. International Journal of Geomechanics 18(12):04018168.
11. U. D. Patil. Characterization of Compacted Silty Sand Using a Double-Walled Triaxial Cell With Fully Automated Relative-Humidity Control[J]. Geotechnical Testing Journal, 2016, 39(5): 742-756.
12. U D. Patil et al. Modeling critical-state shear strength behavior of compacted silty sand via suction-controlled triaxial testing[J]. Engineering Geology, 2017, 231: 21-33.
13. U D. Patil et al. Suction Stress Characteristic Curves of Cohesive-Frictional Soils from Multiple Suction-Controlled Testing Methods[J]. International Journal of Geomechanics, 2020, 20(7).
14. Wang JJ, Hao YZ, Wang TH (2019) Experimental study on structural characteristics of unsaturated compacted loess. Rock and Soil Mechanics 2019(4):1351-1357.
15. Wang J, Zhang D, Wang N, et al (2019) Mechanisms of wetting-induced loess slope failures. Landslides 16(5):937-953.
16. Wen BP, Yan YJ (2014) Influence of structure on shear characteristics of the unsaturated loess in Lanzhou, China. Engineering Geology 168:46-58.
17. Xing X, Li T, Fu Y (2016) Determination of the related strength parameters of unsaturated loess with conventional triaxial test. Environmental Earth Sciences 75(1):82.
18. Xing Y, Gao D, Jin S, et al (2019) Study on Mechanical Behaviors of Unsaturated Loess in terms of Moistening Level. KSCE Journal of Civil Engineering 23(3):1055-1063.
19. Yan CG, Wan Q, Xu Y, Xie Y, Yin P (2018) Experimental study of barrier effect on moisture movement and mechanical behaviors of loess soil. Engineering Geology, 240: 1-9.
20. Yang XH (2008) Study on strength property of unsaturated remolded. Dissertation, Northwest A&F University.
21. Zheng H, Lin H, Zhou W, Bao H, Zhu X, Jin Z, Song Y, Wang Y, Liu W, Tang Y (2019) Revegetation has increased ecosystem water-use efficiency during 2000–2014 in the Chinese Loess Plateau: Evidence from satellite data. Ecological Indicators 102:507-518.

Figures

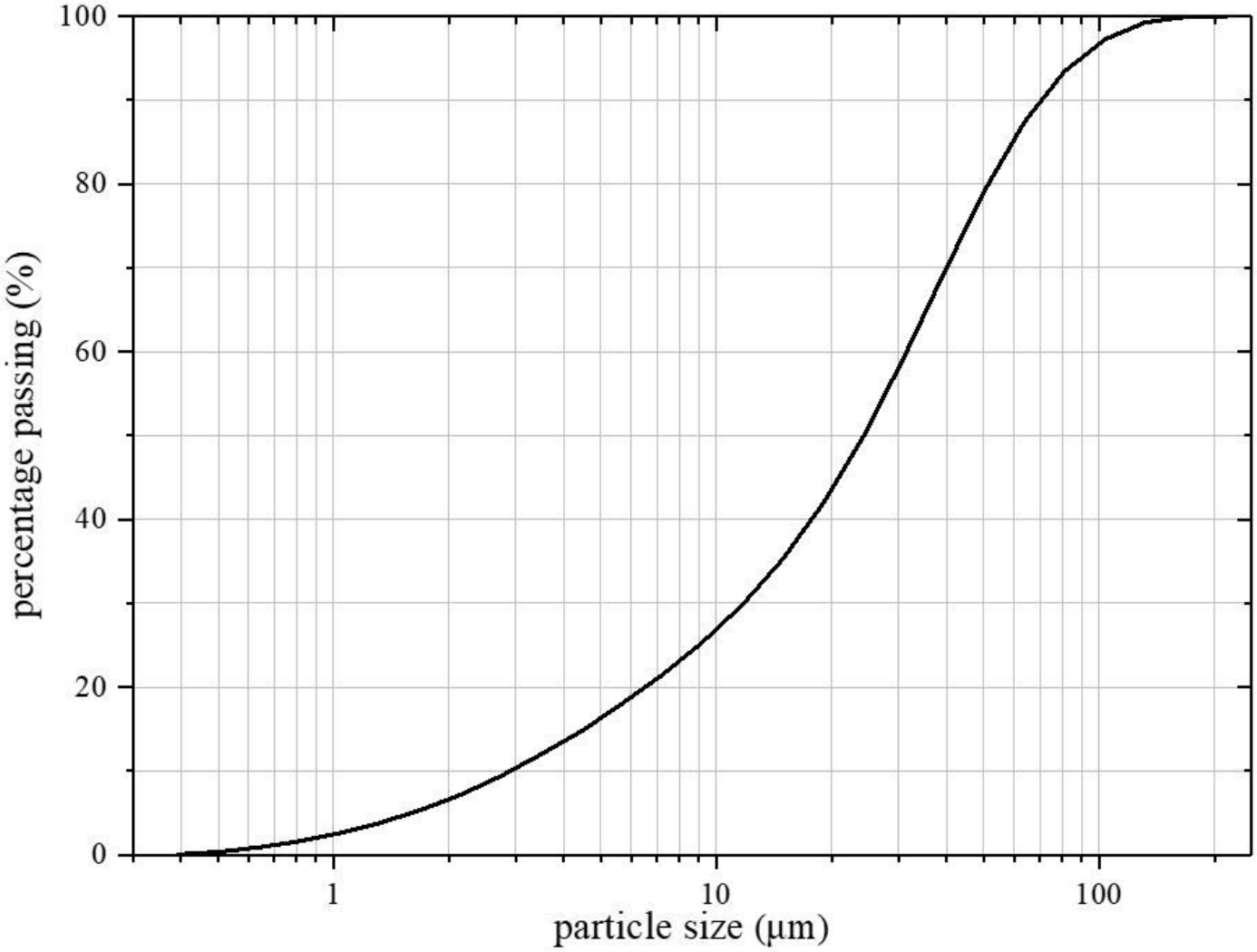

Figure 1

Particle-size distribution of soil

Figure 2

Failure characteristics of soil samples under different confining pressures (ρ_d=1.7g/cm^3, σ_3=50kPa, 100kPa, 150kPa, 200kPa)

(on the far left is the untested sample, with progressively increasing confining pressure from left to right)

Figure 3

Failure characteristics of soil samples at different dry densities (ω=10%,ρ_d=1.4g/cm^3, 1.5g/cm^3, 1.6g/cm^3, 1.7g/cm^3)

(on the far left is the untested sample, and the dry density increases step by step from left to right)

Figure 4

Failure characteristics of soil samples with different water content (σ_3=50kPa, ω=10%, 15%, 20%, 25%)

(on the far left is the untested sample, and the moisture content increases step by step from left to right)

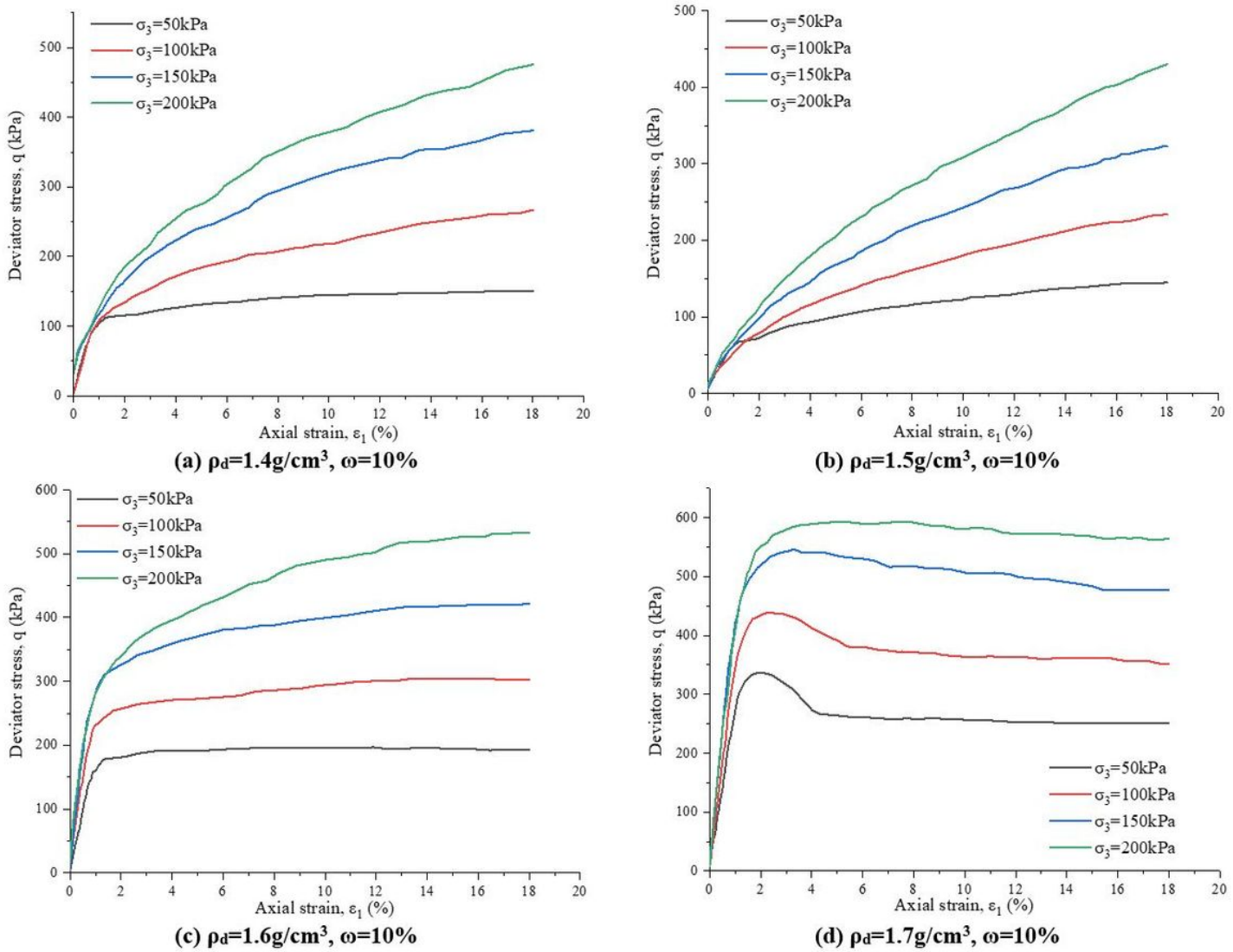

Figure 5

Stress-strain curves under different confining pressures

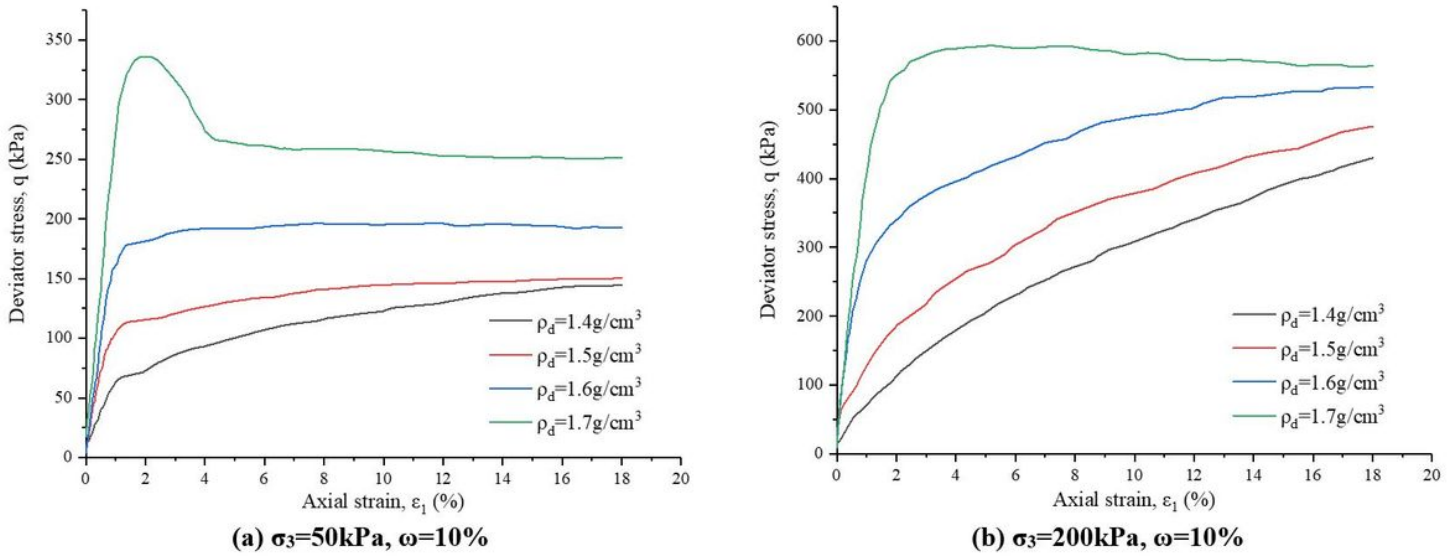

Figure 6

Stress-strain curves under different dry densities

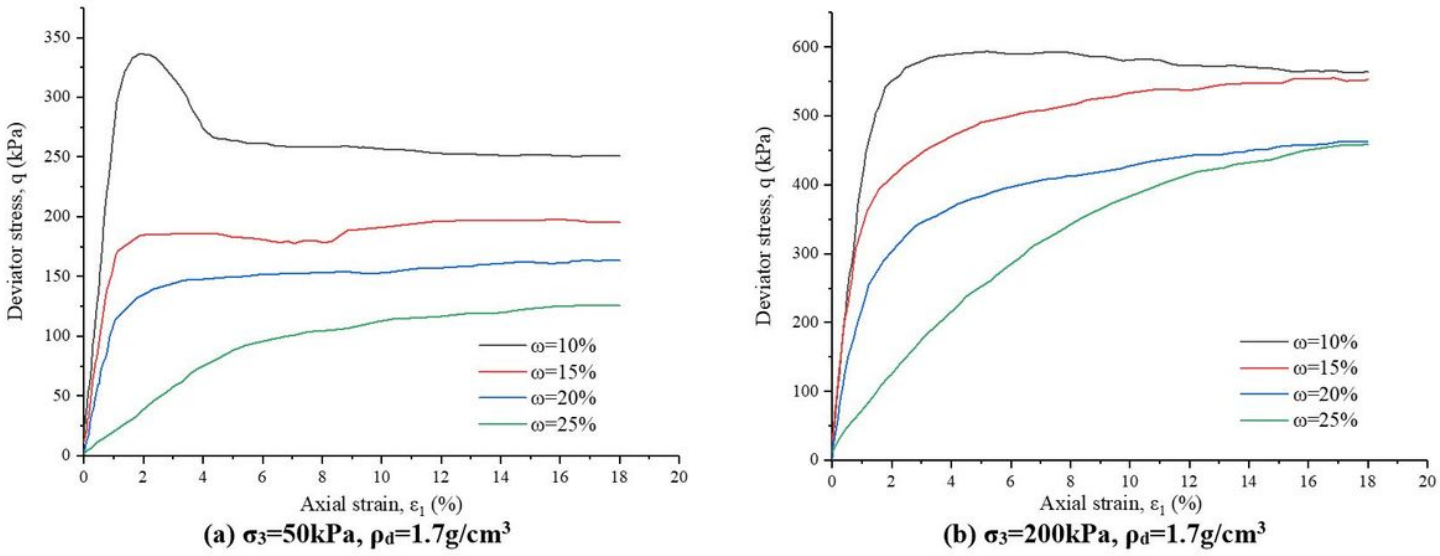

Figure 7

Stress-strain curve under different moisture content

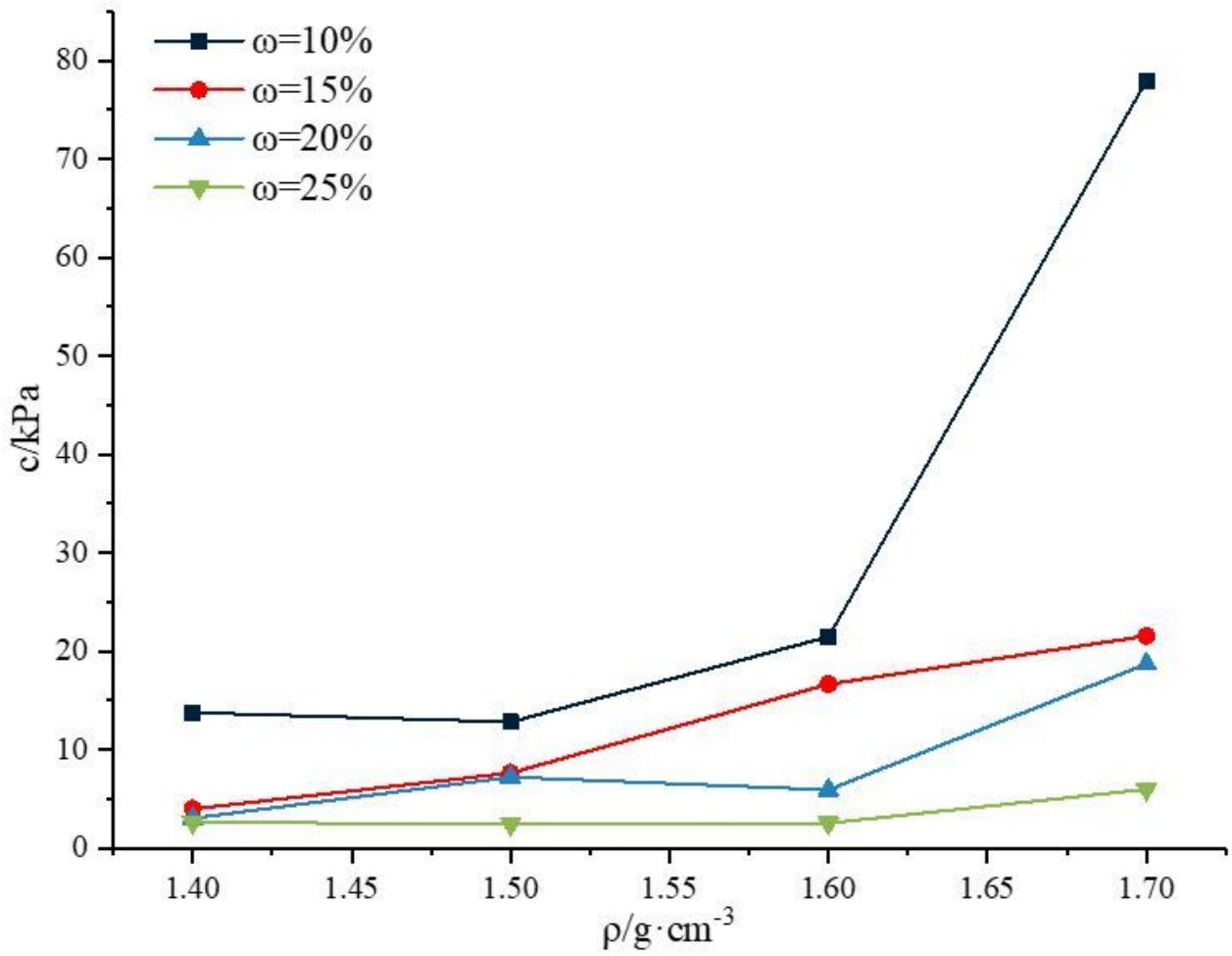

Figure 8

The variation rule of cohesion under different water content

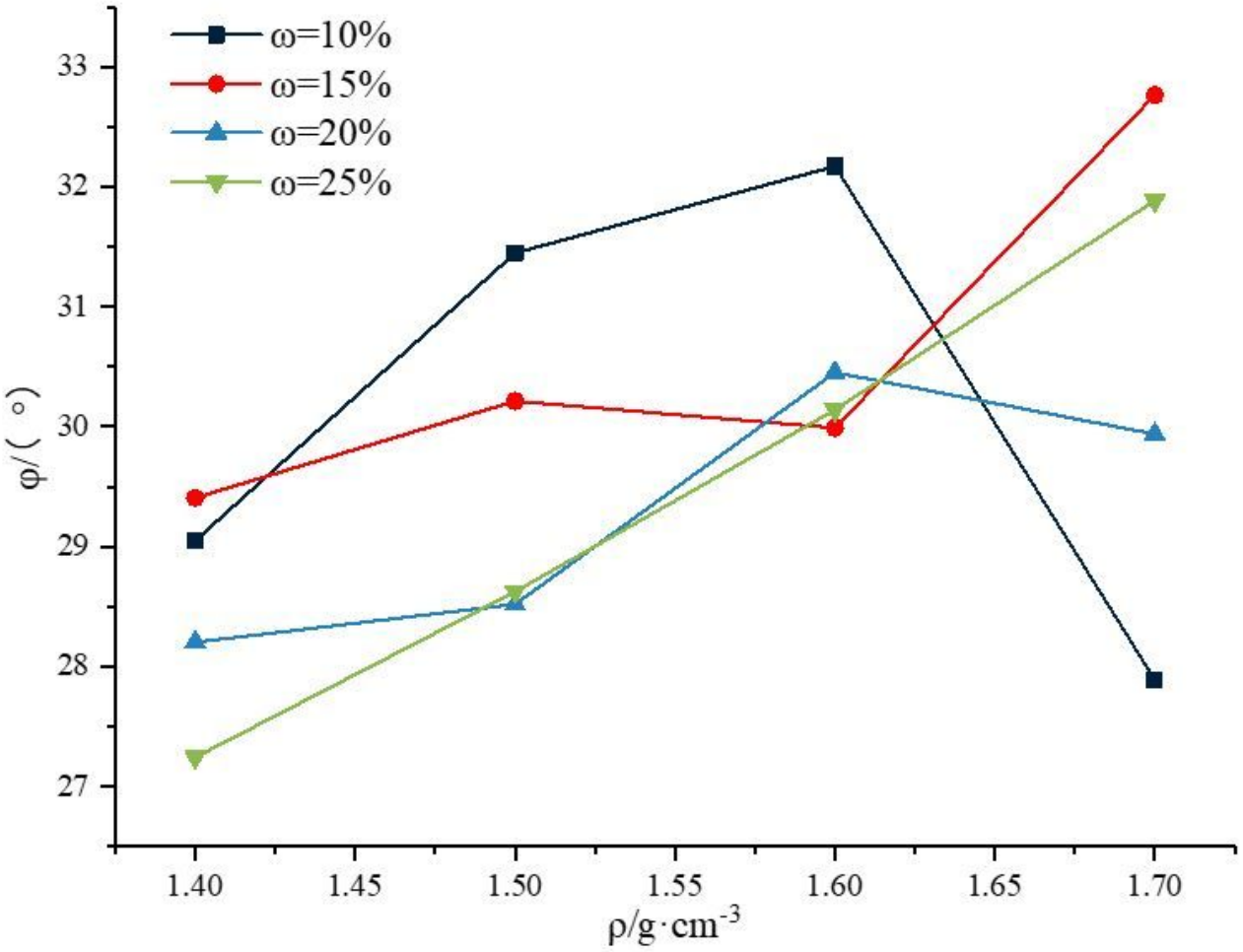

Figure 9

The variation law of internal friction Angle under different water content

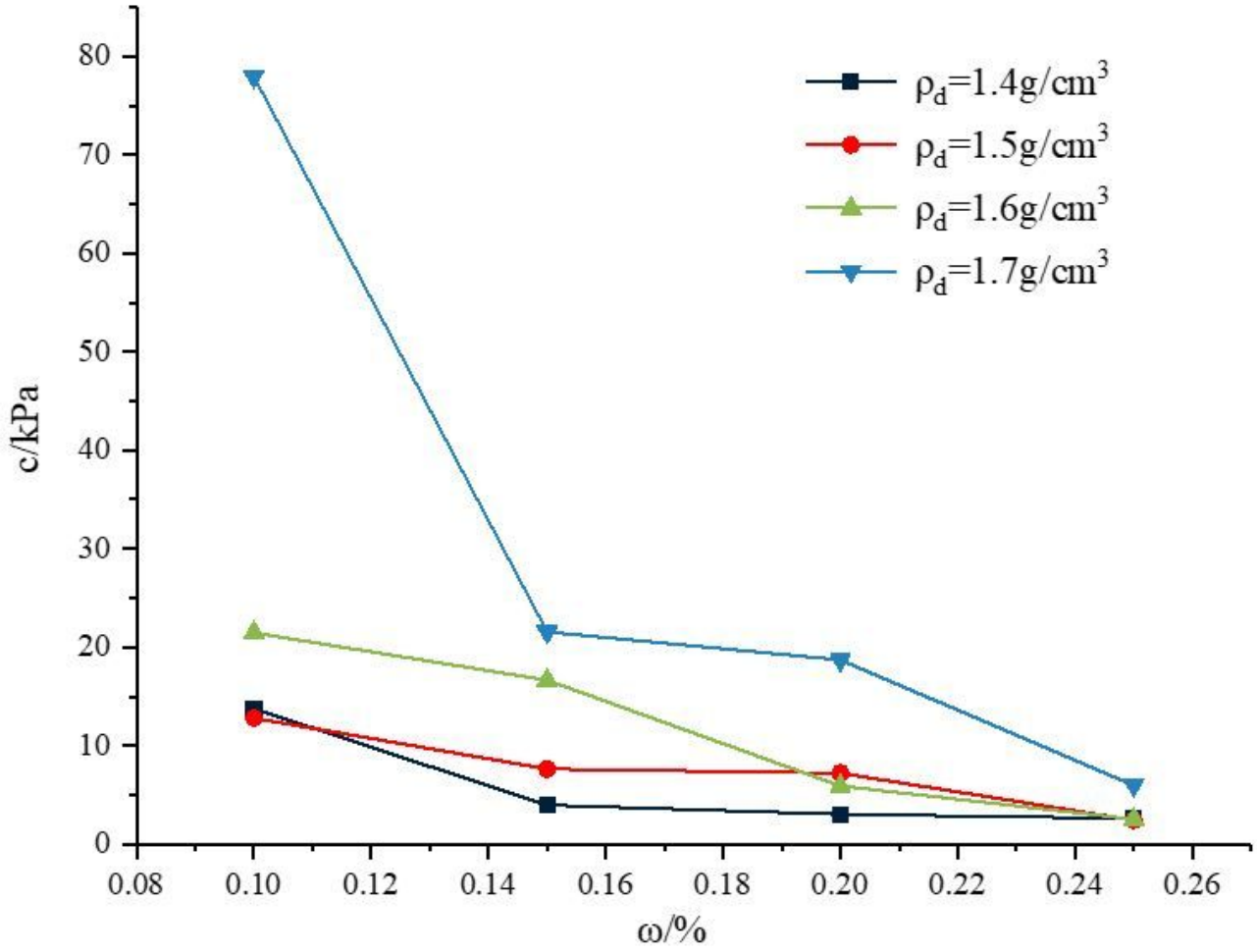

Figure 10

The variation rule of cohesion under different dry density

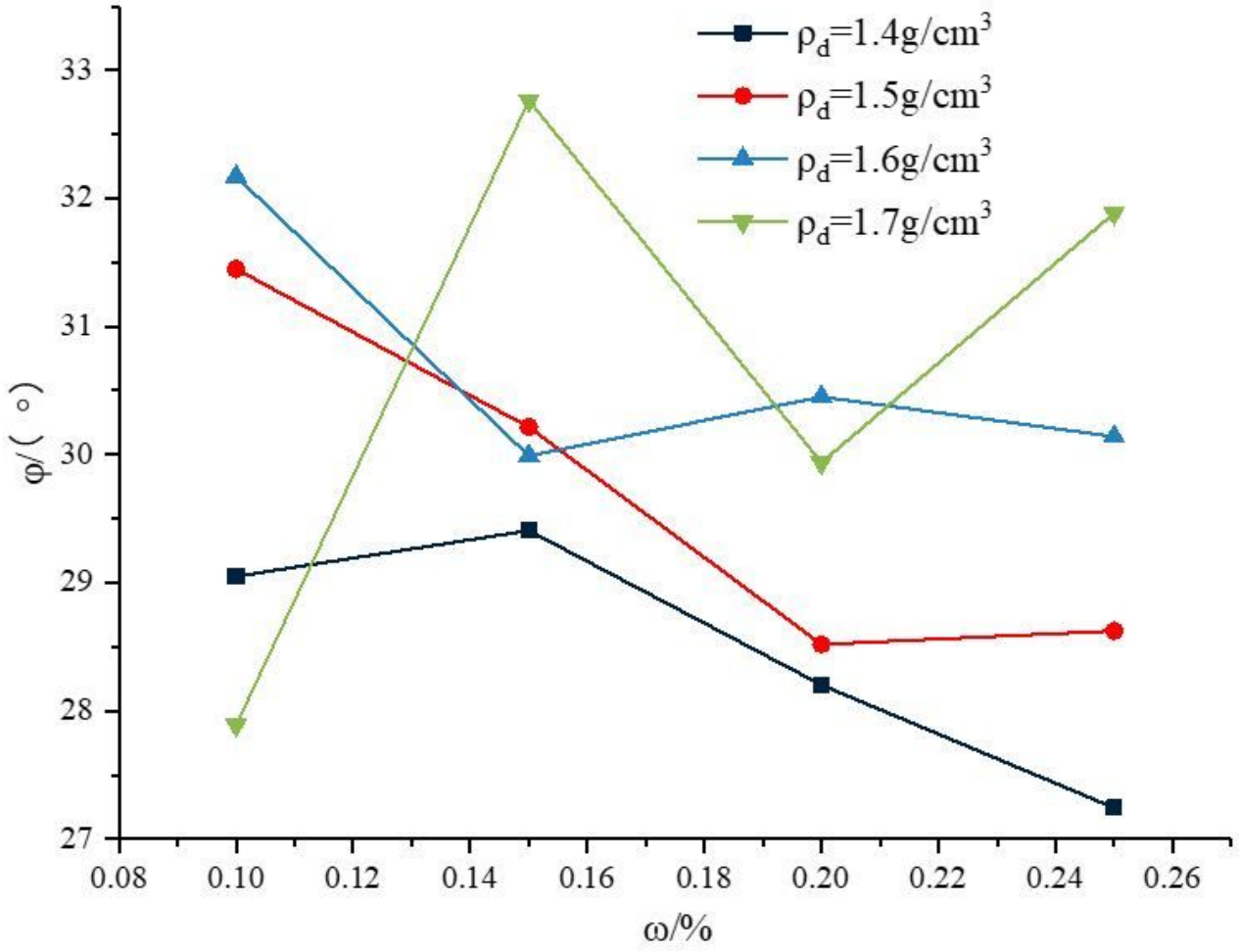

Figure 11

The variation law of internal friction under different dry density

Figure 12

Loess stacking dam

Figure 13

Photograph of the front damage

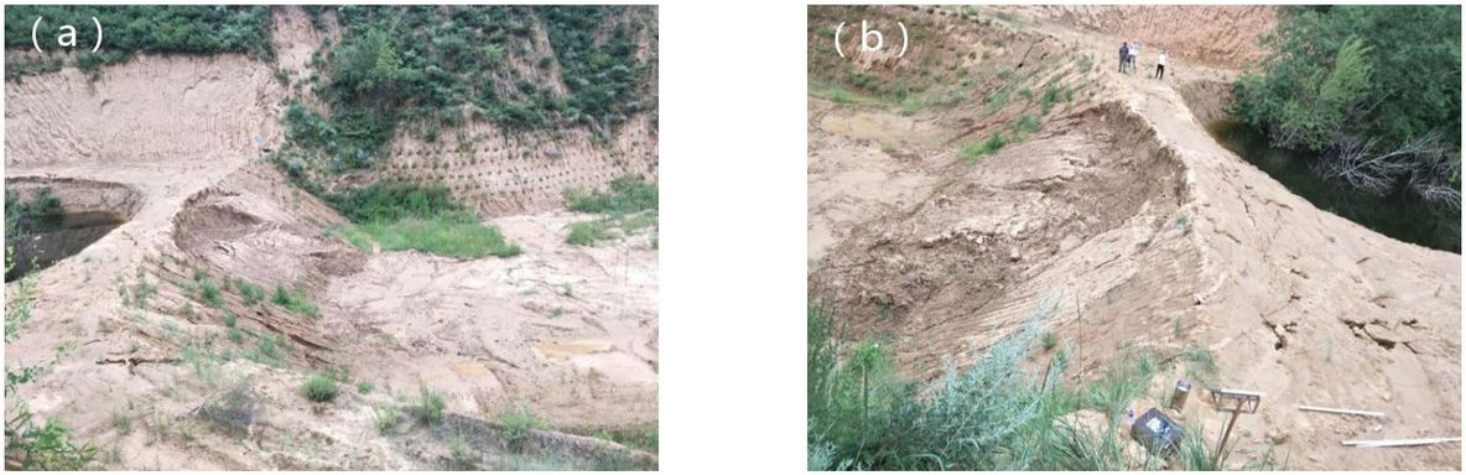

Figure 14

First instance of dam damage

Figure 15

Second instance of dam damage

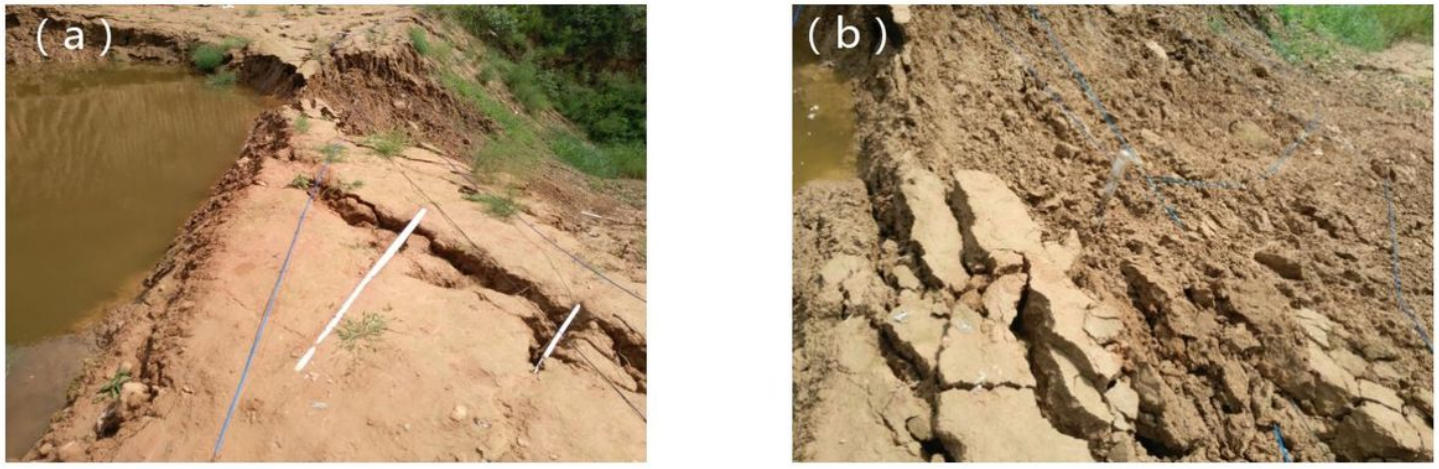

Figure 16

Third instance of dam damage

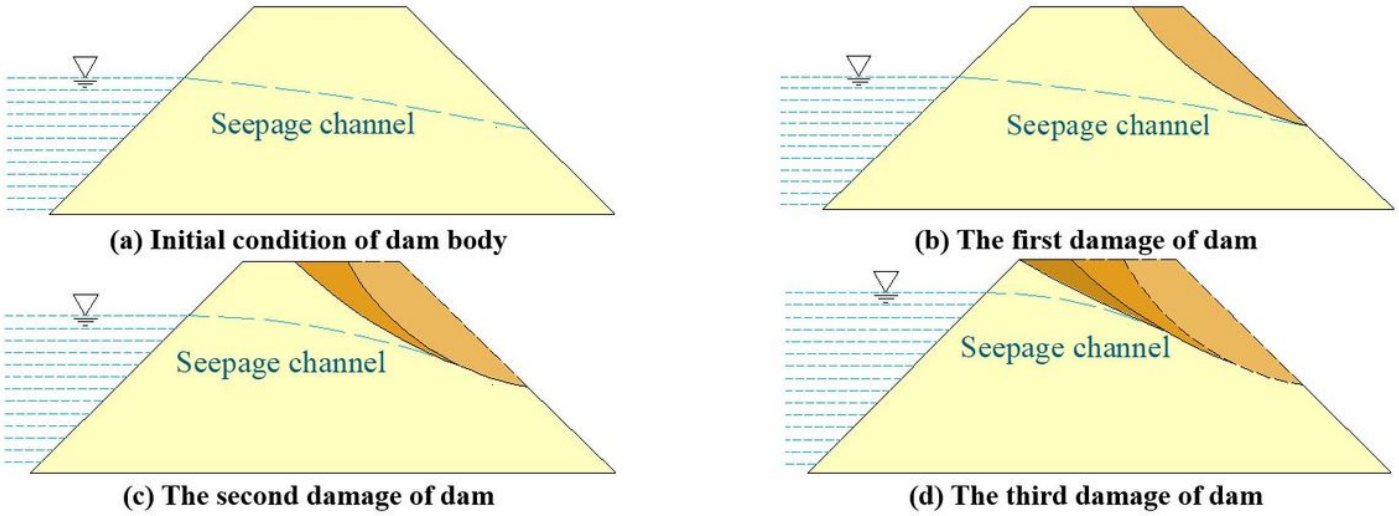

Figure 17

Seepage progressive failure process of loess stacking dam

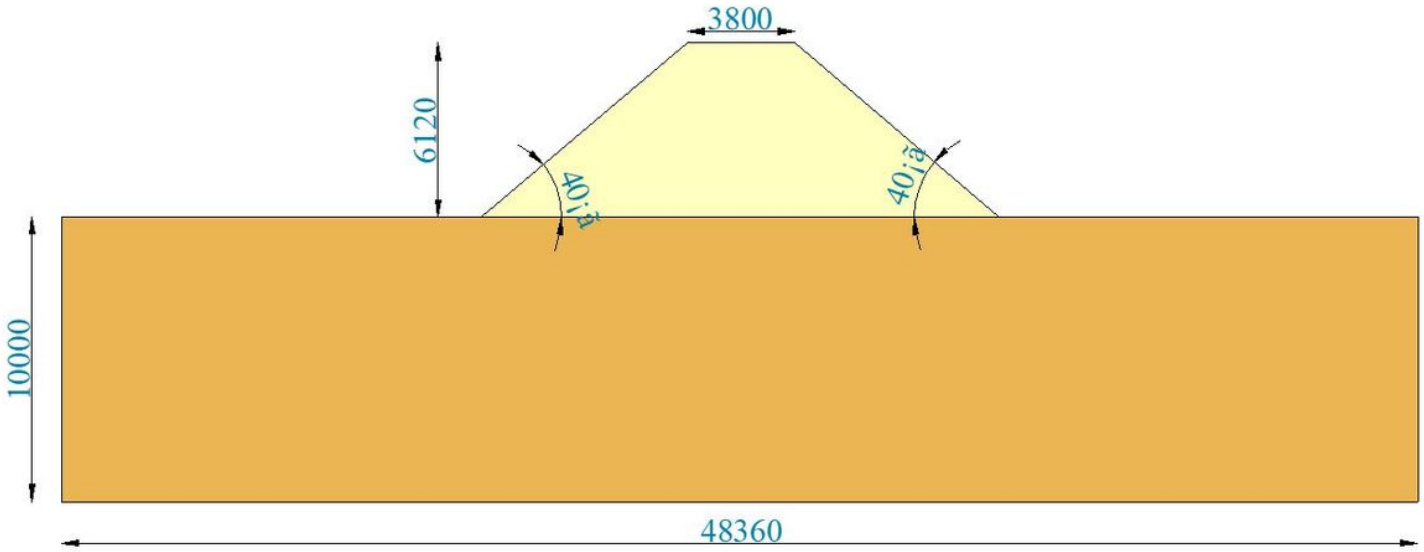

Figure 18

calculation model

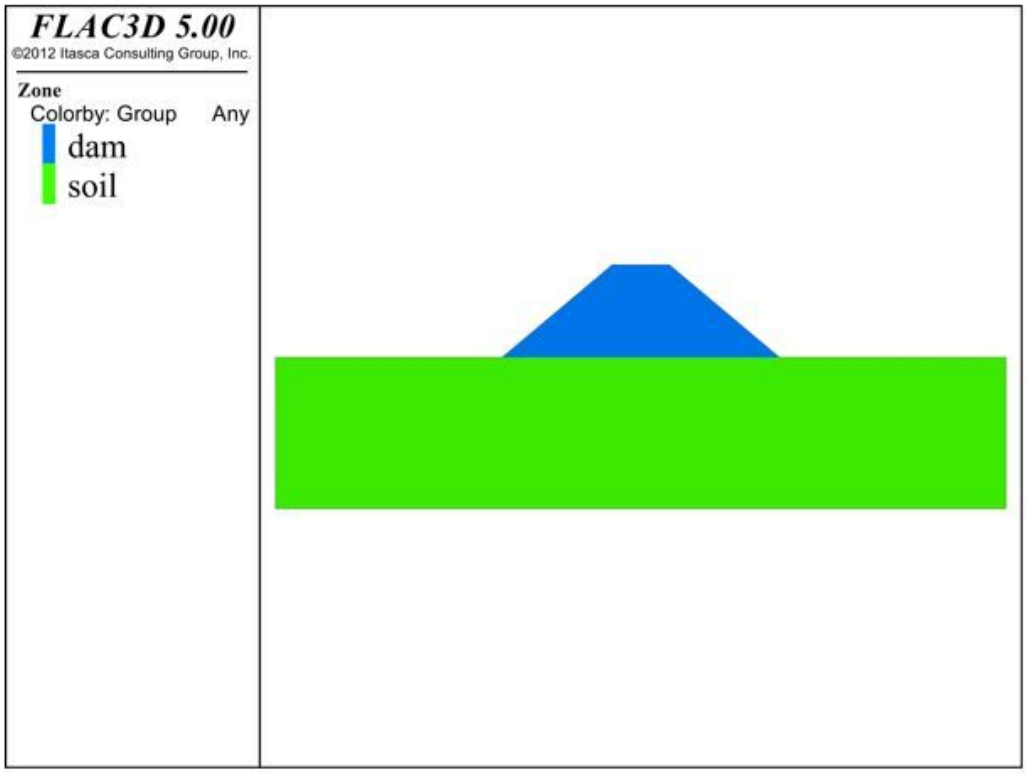

Figure 19

Initial calculation model

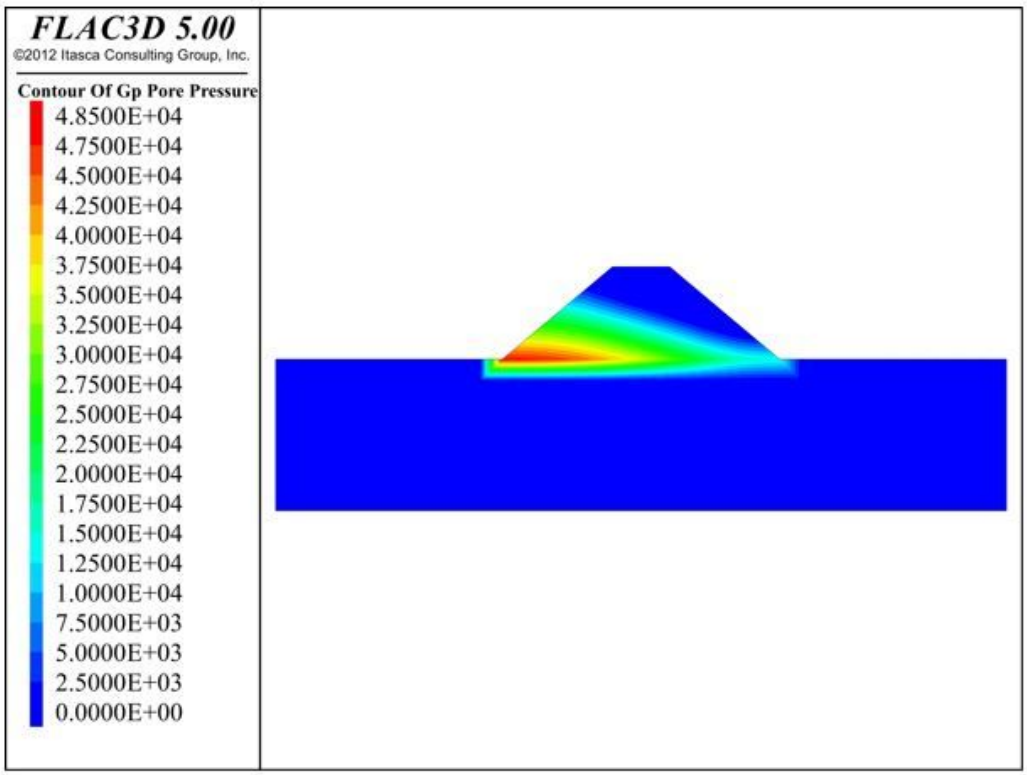

Figure 20

The first damage of pore pressure cloud chart

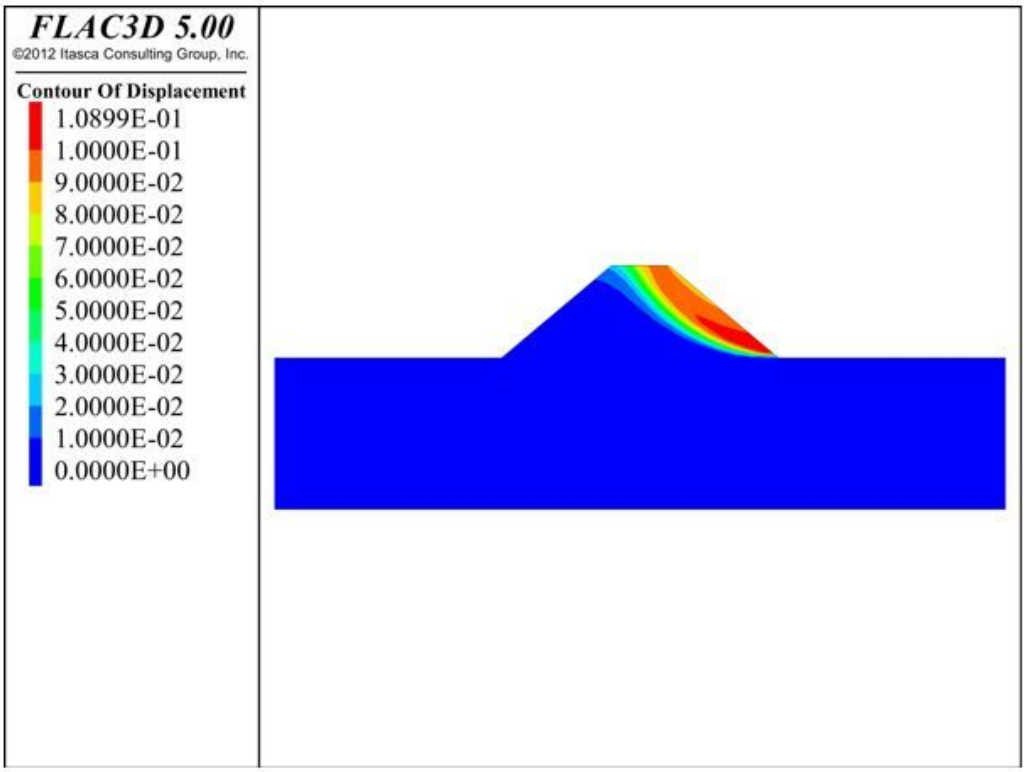

Figure 21

The first damage of displacement cloud chart

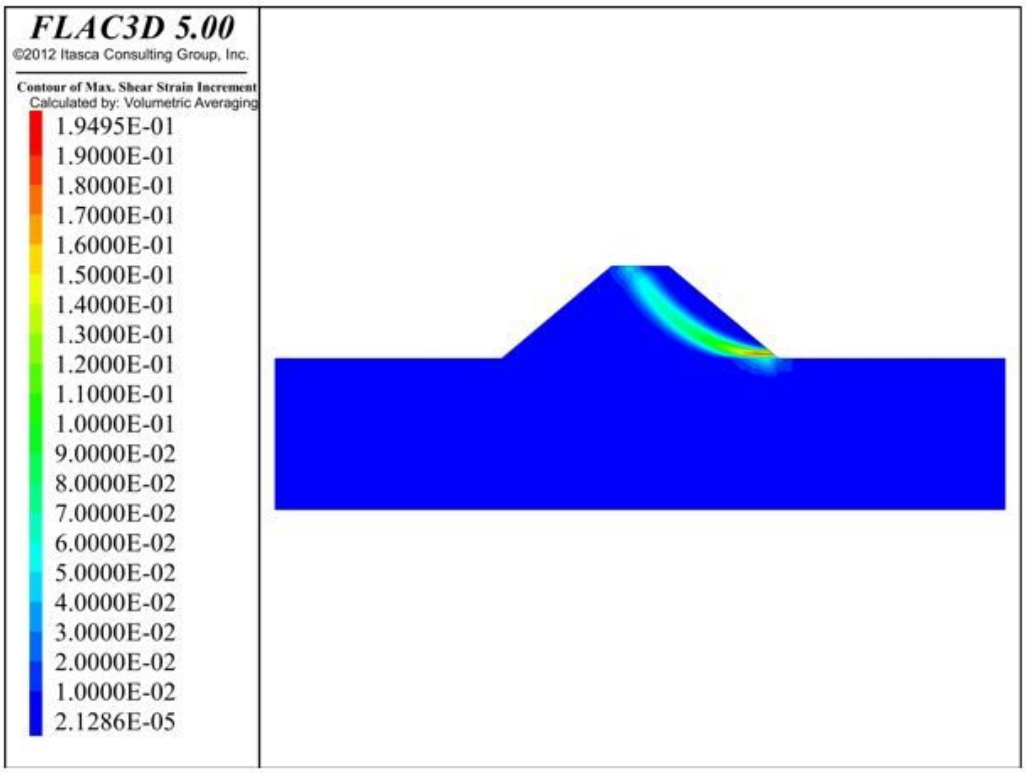

Figure 22

The first damage of maximum shear strain increment cloud chart

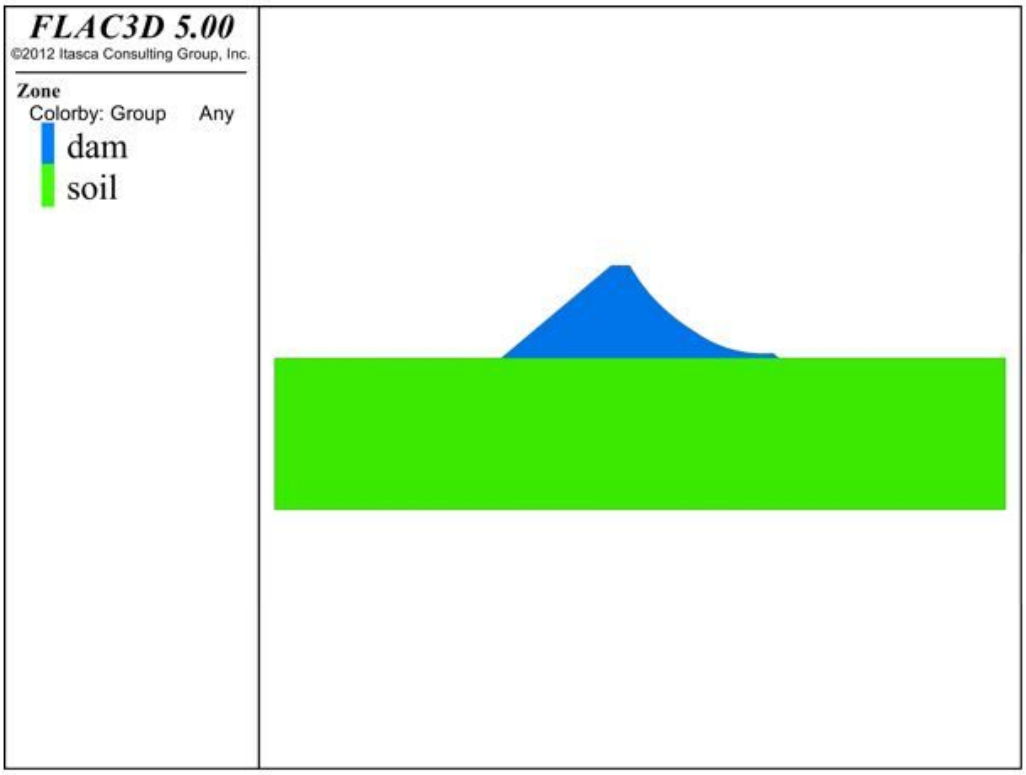

Figure 23

The second damage of calculation model

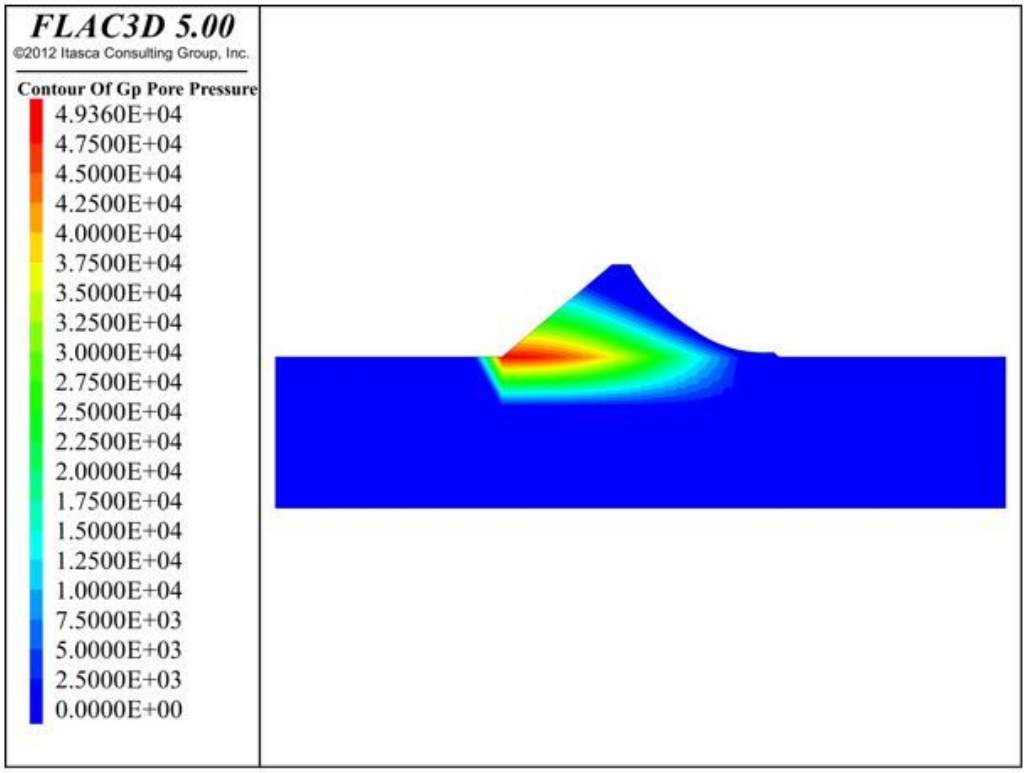

Figure 24

The second damage of pore pressure cloud chart

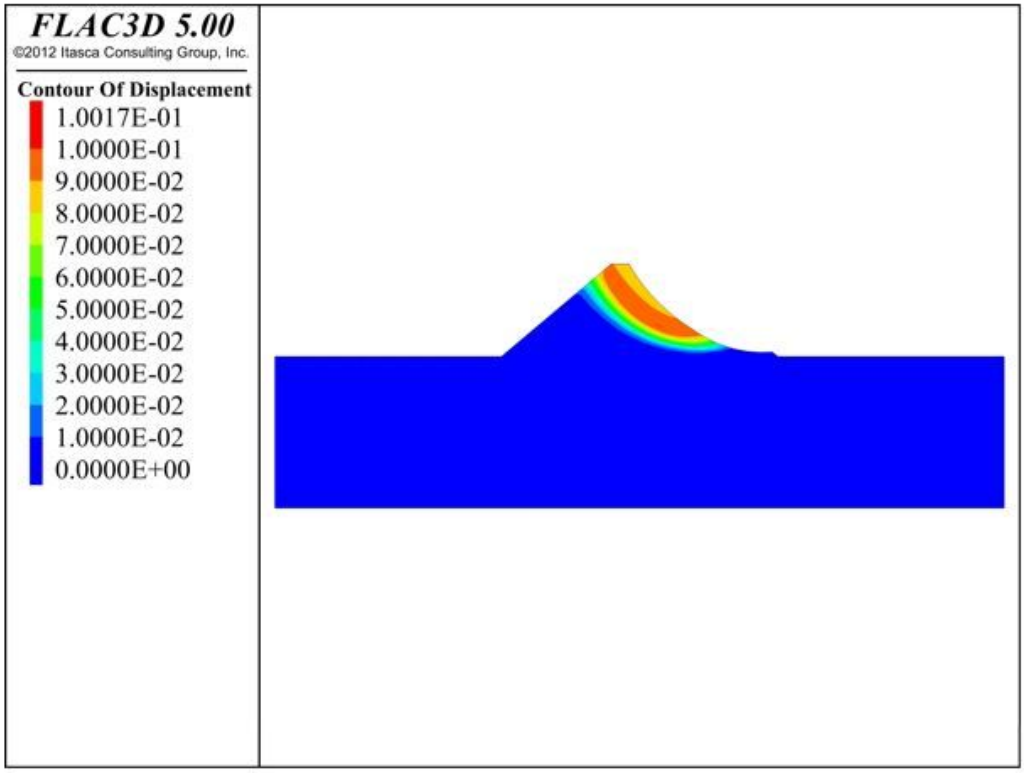

Figure 25

The second damage of displacement cloud chart

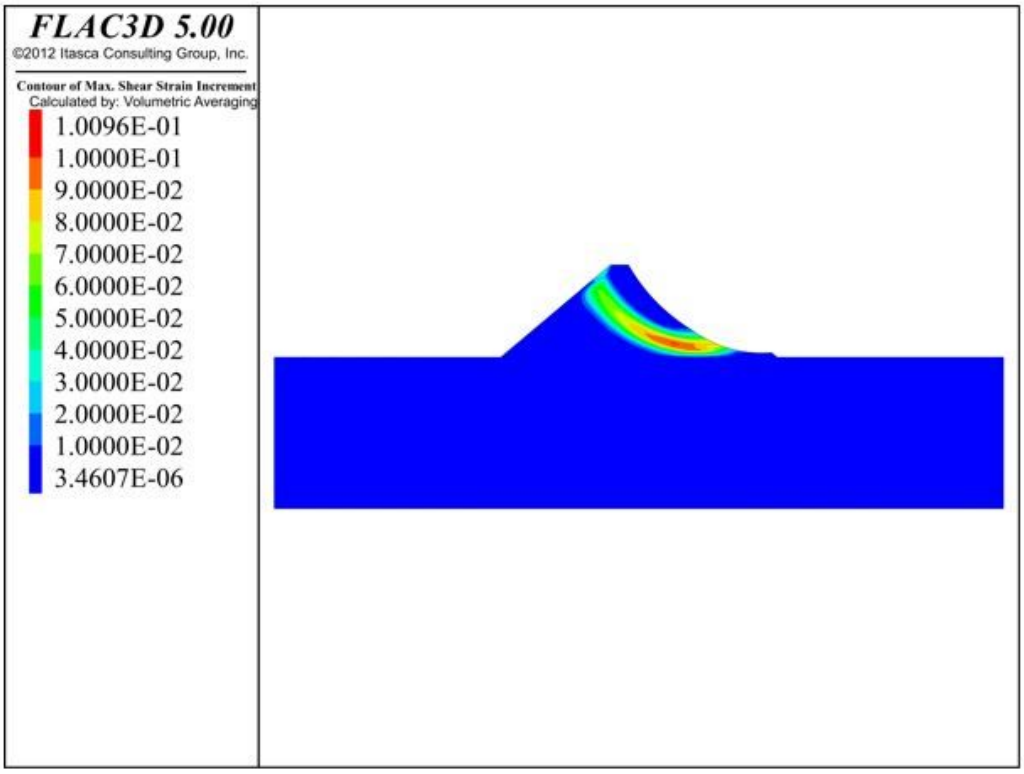

Figure 26

The second damage of maximum shear strain increment cloud chart

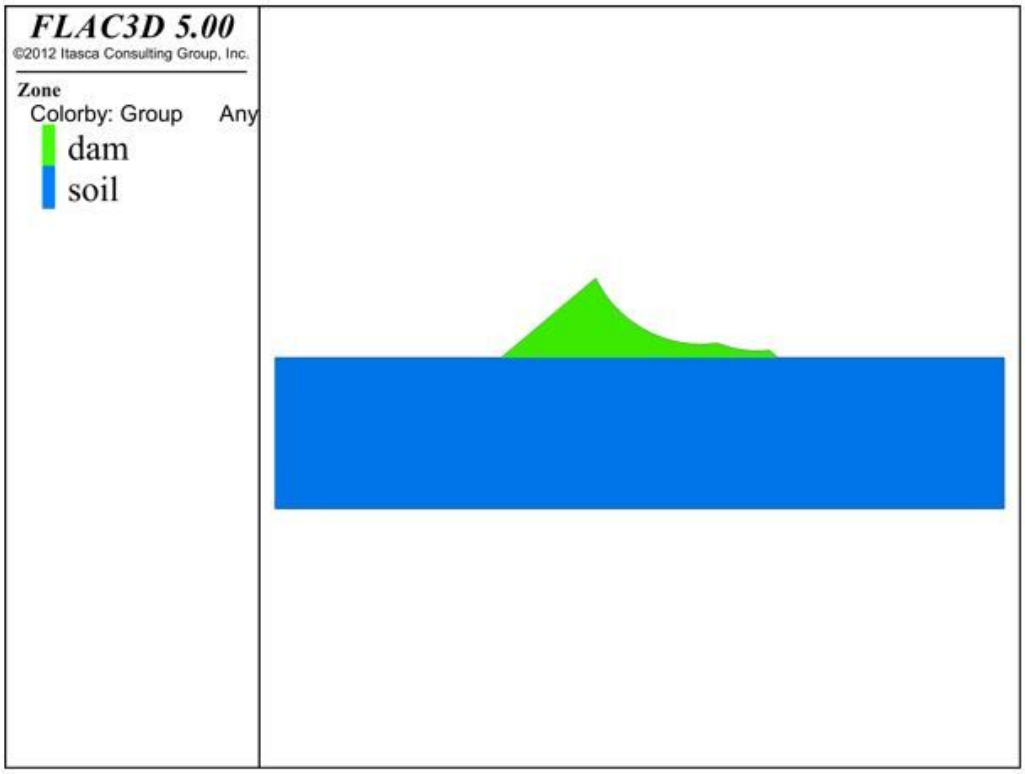

Figure 27

The third damage of calculation model

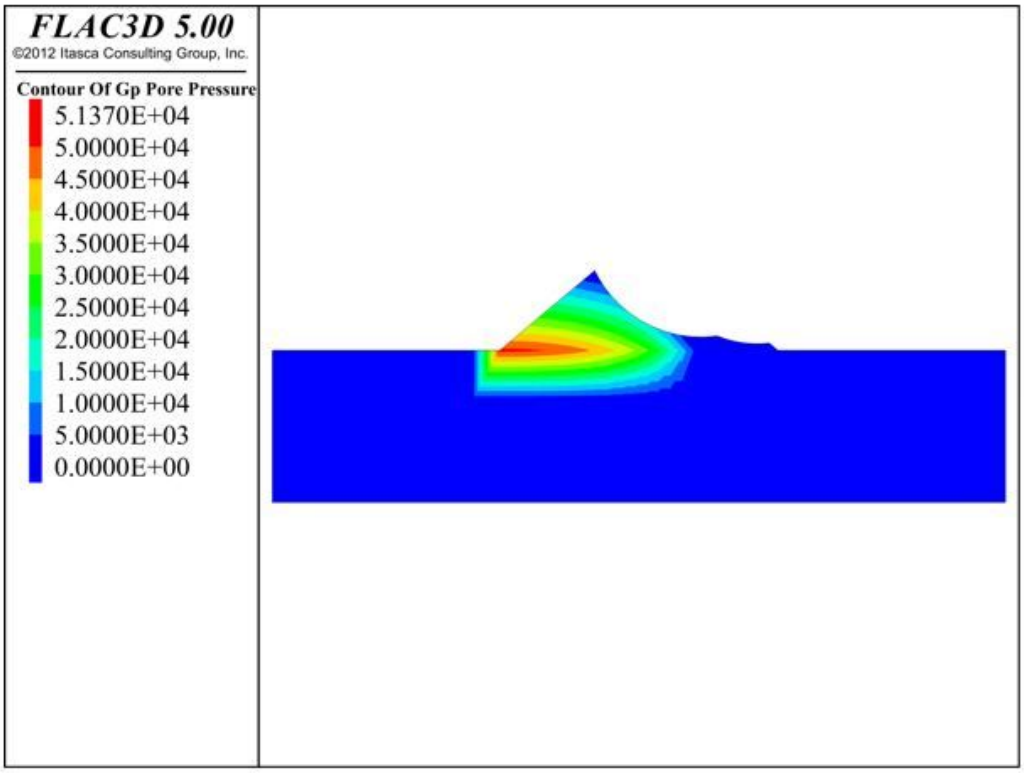

Figure 28

The third damage of pore pressure cloud chart

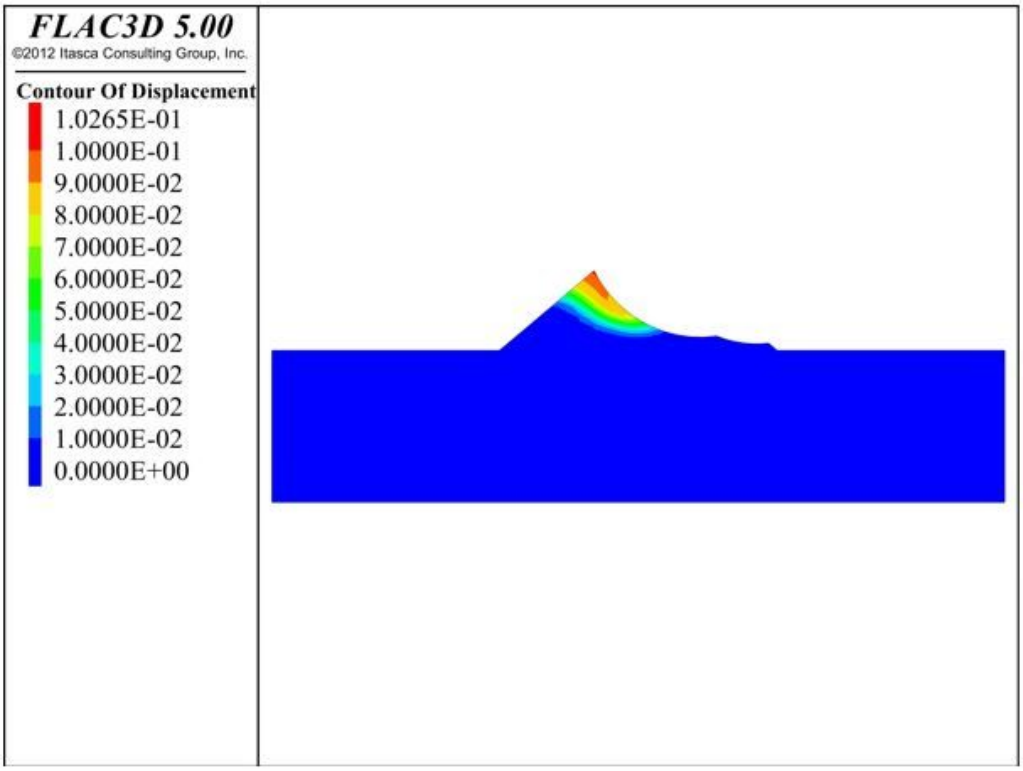

Figure 29

The third damage of displacement cloud chart

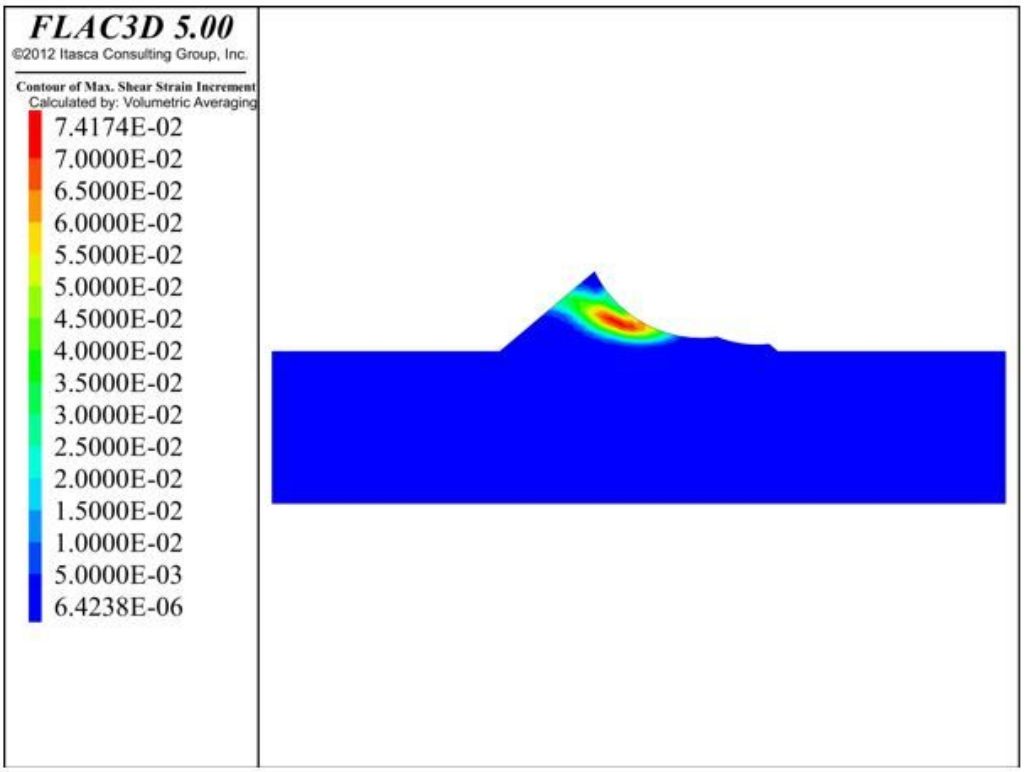

Figure 30

The third damage of maximum shear strain increment cloud chart